Specification and design for full energy beam exploitation of the compact linear accelerator for research and applications

E. W. Snedden[*] D. Angal-Kalinin, A. R. Bainbridge, A. D. Brynes,[†] S. R. Buckley,
D. J. Dunning, J. R. Henderson, J. K. Jones, K. J. Middleman, T. J. Overton, T. H. Pacey,
A. E. Pollard, Y. M. Saveliev, B. J. A. Shepherd, and P. H. Williams

*Accelerator Science and Technology Centre (ASTeC), STFC Daresbury Laboratory, Keckwick Lane,
Warrington, WA4 4AD, United Kingdom and Cockcroft Institute,
Keckwick Lane, Warrington, WA4 4AD, United Kingdom*

M. I. Colling, B. D. Fell, and G. Marshall
*Technology Department, STFC Daresbury Laboratory,
Keckwick Lane, Warrington, WA4 4AD, United Kingdom*

The compact linear accelerator for research and applications (CLARA) is a 250 MeV ultrabright electron beam test facility at STFC Daresbury Laboratory. A user beamline has been designed to maximize the exploitation of CLARA in a variety of fields, including novel acceleration and new modalities of radiotherapy. In this paper, we present the specification and design of this beamline for full energy beam exploitation. We outline the key elements that will provide users access to ultrashort, low emittance electron bunches in two large experiment chambers. The results of start-to-end simulations are reported that verify the expected beam parameters delivered to these chambers. Key technical systems are detailed, including those which facilitate a combination of electron bunches with high-power laser pulses.

I. INTRODUCTION

The compact linear accelerator for research and applications (CLARA) is an ultrabright electron beam test facility at STFC Daresbury Laboratory. The facility was conceived to test advanced free-electron laser (FEL) schemes that could be implemented on existing and future short-wavelength FEL facilities [1].

A schematic of the CLARA facility is shown in Fig. 1. The CLARA front end, producing 50 MeV, 250 pC electron bunches from a 10 Hz S-band photoinjector gun and linac, was successfully commissioned in 2018 [2]. Installation of accelerator modules to raise the beam energy to 250 MeV will be completed by the end of 2023. The front-end photoinjector gun will be replaced with a novel 100 Hz high repetition rate gun (HRRG) [3], which has been commissioned on an adjacent beamline. The remaining beamline consists of three 4-m S-band (2998.5 MHz)

linacs, X-band fourth harmonic cavity (4HC) phase space linearizer, dielectric dechirper, variable magnetic bunch compressor (VBC), and a dedicated diagnostics line. The diagnostic line includes a transverse deflecting cavity (TDC), which when combined with 4D transverse emittance measurements, allows for 6D characterization. The original CLARA concept included a laser heater [4] (which can be installed in future if required) and reserved space within the electron hall for a seeded FEL, including seeding laser, modulators, undulators, and photon diagnostics; although the FEL has not been funded, the space has been reserved for future applications.

Beginning in 2018, access to electron beams from the CLARA front end has been made available to users from academia and industry. This has enabled the testing of novel concepts and ideas in a wide range of disciplines, including the development of advanced accelerator technology [5], medical applications [6], novel particle beam acceleration [7], and deflection [8,9] concepts.

Based on increasing user demand for access, a decision has been made to design and build a dedicated beamline for user applications at the full CLARA beam energy of 250 MeV. As shown in Fig. 1, the beamline for full energy beam exploitation (FEBE) will be installed parallel to the space originally allocated for an FEL.

There are only a handful of test facilities worldwide that provide user access to midenergy range (less than

---
[*]edward.snedden@stfc.ac.uk

[†]Present address: Elettra-Sincrotrone Trieste S.C.p.A, 34149 Basovizza, Italy.
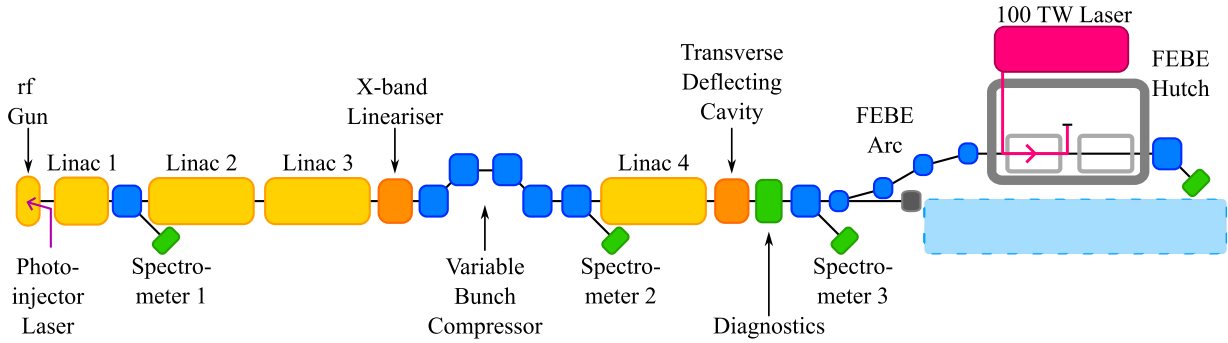
FIG. 1.   Schematic of the CLARA linear accelerator test facility, including the FEBE beamline, shielded FEBE hutch, 100 TW laser system, and space reserved for potential future applications (shaded blue area).

300 MeV), high-brightness electron beams to test proof of principle novel applications. A survey of beam dynamics challenges of such midenergy high-brightness facilities in Europe has recently been carried out and was presented at IPAC-2023 [10]. In addition to CLARA, there are three other facilities in Europe; CLEAR@CERN [11,12], ARES@DESY [13,14], and SPARC_LAB@INFN [15] in this energy range.

The CLEAR facility provides bunch trains of beam energy up to 230 MeV at a maximum repetition rate of 10 Hz; the number of microbunches in each train can be varied from 1 to 150 with spacing of 1.5 or 3 GHz, and bunch charge can be varied from 5 pC to 3 nC. The ARES facility provides single bunches up to 160 MeV at a maximum repetition rate of 50 Hz, and bunch charge can be varied from 3 fC to 280 pC. The SPARC_LAB facility provides single bunches up to 180 MeV at a maximum repetition rate of 10 Hz, and the bunch charge can be varied from 10 pC to 2 nC. In addition to CLARA, SPARC_LAB is the only test facility with access to a high-power laser (FLAME [16], 250 TW) to allow combined electron-laser experiments.

A survey of CLARA stakeholders was performed to inform the design of the new beamline, and the results of this survey identified three key design principles: (i) FEBE should provide access to a dedicated shielded experiment area ("hutch"), accessible to users without switching off CLARA. (ii) The hutch should incorporate large experiment chambers compatible with a wide range of possible experiments. (iii) The beamline should allow the synchronized interaction of electron bunches with a high-power ($\sim$100 TW) laser.

The decision to provide a dedicated shielded hutch was taken following consultation with other medium-energy accelerator facilities. This arrangement allows on-demand user access to the experimental area without fully switching off the accelerator, which reduces disruption, improves machine stability, and allows experiments to resume promptly after access. This type of access is not currently possible at other similar facilities in Europe, although CLEAR has developed robotic systems to minimize user access requirements during some types of experiments.

In this article, we report on the specification and design of the FEBE beamline, which is currently under construction and will begin commissioning in 2024. The article is broken down as follows: the layout of the machine and beam specification are presented in Sec. II; Sec. III reports the results of beam dynamics simulations from the CLARA photoinjector through to the FEBE beam dump; and Sec. IV details the key technical accelerator systems expected to underpin future user exploitation. The article concludes with a summary in Sec. V.

II. LAYOUT AND BEAM SPECIFICATION

FEBE has been designed to support a variety of experiments across the fields of accelerator applications and accelerator technology. A user survey performed in 2018 established a particular interest in the exploitation of novel acceleration research and development (R&D) including: External injection of electron bunches into a plasma accelerator stage (using both beam- and laser-driven configurations); structure wakefield acceleration, encompassing the use of metallic, dielectric, and novel (e.g., metamaterial or photonic crystal based) structures; and dielectric laser acceleration, including both direct optical laser coupling to a solid structure or prior conversion to longer wavelength (THz band).

The requirements of novel acceleration techniques have been identified as the most challenging of the anticipated user requests and have been used to drive the FEBE beam specification and underpinning accelerator technology (the latter outlined in Sec. IV). Characteristics of electron drive beams required for novel acceleration include high peak currents (order 1 kA) [17], short bunch lengths (order 10 fs), and small transverse beam sizes ($<$10 μm) [18]. More demanding experiments and applications may require a combination of multiple characteristics simultaneously [19]. To verify and optimize the various acceleration techniques, diagnostics for the characterization of electron bunches both before and after interactions are required [20].

FEBE also expects to host a variety of target irradiation experiments, including R&D in very high electron energy
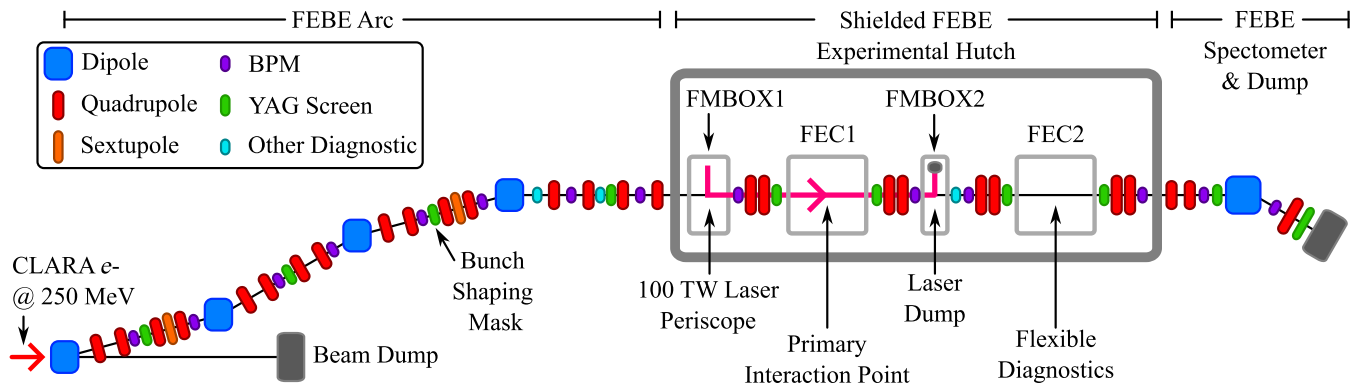
FIG. 2.   Schematic of the new beamline for full energy beam exploitation (FEBE), including arc (connecting to the upstream CLARA main beamline, Fig. 1), experiment hutch, and posthutch beam dump with energy and emittance diagnostics.

(VHEE) therapy, radiation generation, and electron detectors. This is a broad category and experiment chambers must be suitably flexible to accommodate a wide variety of samples (both vacuum and in air), with suitable motion control for accurate positioning and installation of beryllium windows for in-air experiments. Diagnostics to validate beam parameters delivered to the target are also required.

A schematic of the FEBE beamline is shown in Fig. 2 and is broken down into three sections: an arc and matching section connected to the main CLARA beamline; the FEBE experiment hutch, which brings the electron beam to a focus at two possible interaction points (IPs); and posthutch transport line and beam dump. The FEBE experiment hutch is a $10 \times 5.4 \times 3$ m^3 dedicated area for users to perform electron beam experiments.

The hutch is transversely offset from the main CLARA beamline using a FODO structure to provide -I transform between two dipoles (dipole angles of 14°) and optimized to minimize emittance growth due to coherent synchrotron radiation (CSR) [21]. This solution leads to a strong focusing, achromatic, and nonisochronous arc with large natural second-order longitudinal dispersion, requiring correction by sextupole magnets at positions of high dispersion. Six quadrupole families allow matching to the main beamline for a range of electron beam configurations. The arc has a nominal R_{56} value of 7.7 mm with no residual dispersion. Longitudinal bunch compression of the electron beam within the hutch can be achieved using a combination of the FEBE arc and the upstream VBC.

The FEBE arc includes a mask array positioned at a point of high dispersion for shaping the bunch longitudinal distribution, including generation of drive/main bunch pairs with variable delay; a single ultrashort (order 1 fs duration) low charge bunch; and, as shown in Fig. 3, a drive bunch with a train of witness bunches. The mask is made from 5 mm tungsten and can be changed to meet user requirements. Alternatively, multiple electron bunches can be generated at the photocathode via manipulation of the photoinjector laser, before acceleration and transport to FEBE.

The beam transport is designed to deliver a strong focus to two possible IPs (IP1/2), each located within a large-volume ($\sim$2 m^3) experiment chamber designated FEBE Experiment Chamber (FEC) 1/2. The double-IP design provides flexibility in experiment design and implementation. For example, the interaction between the electron beam and laser generated in FEC1 can be captured and probed with beam diagnostics installed in FEC2. The design also allows multiple independent experiments to be installed in FEC1 and FEC2 where compatible, minimizing downtime for setup, with each chamber, expected to achieve nominal vacuum with approximately 1 h pumping.

To meet novel acceleration requirements, FEC1 includes the capability to combine electron beams with high-power lasers at the IP. The laser is introduced into the beamline in a dedicated mirror box, whereupon it can be transported directly to FEC1 or focused and co-propagated (using a $\sim$3.5 m effective focal length off-axis parabola) with the electron beam to the IP. A second transport line bypassing the off-axis parabola and connecting to FEC1 allows shorter focusing geometries to be generated directly within the chamber. A downstream mirror box is used to separate and dump the laser following interaction with the electron beam.
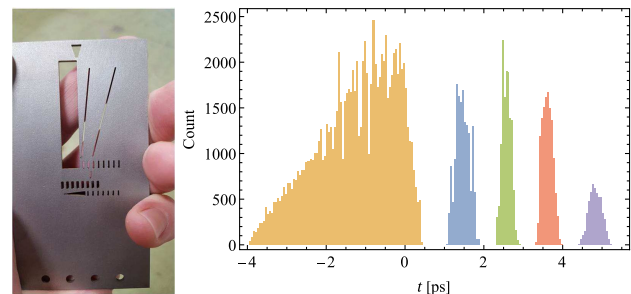

FIG. 3.   Left: photograph of the mask to be installed in FEBE for variable longitudinal shaping. Right: simulated 250 pC longitudinal profile at the FEBE FEC IP using the bottom hole of the mask, including triangular drive bunch ($\sim$1 ps rms) and four trailing bunches ($\sim$100 fs rms duration with 1 ps separation).

TABLE I. FEBE beam parameters at the FEC1 IP. All beam parameters are specified for 250 MeV. Symbol σ_i indicates rms value; $\epsilon_{N,i}$: normalized projected rms emittance. Parameters for initial commissioning and those targeted thereafter following required periods of machine development are presented.

Parameters	Commissioning		Machine development	
	High charge	Low charge	High charge	Low charge
Charge (pC)	250	5	250	5
σ_t (fs)	100	50	≤ 50	$\ll 50$
σ_x (µm)	100	20	50	~ 1
σ_y (µm)	100	20	50	~ 1
σ_E (%)	<5	<1	1	0.1
$\epsilon_{N,x}$ (µm rad)	5	2	<5	<1
$\epsilon_{N,y}$ (µm rad)	5	2	<1	<1

Further detail on the laser system and laser transport is given in Sec. IV. Apertures throughout the beamline must accept both the high-power laser and the electron beam. This includes, for example, the four quadrupoles around FEC1, which must be both a large aperture (radius ∼68 mm) and a high gradient to achieve a tight focus at the IP.

Some experiments (e.g., novel acceleration including plasma and dielectric) will aim to produce beams of energy greater than 250 MeV. All post-FEC1 magnets are, therefore, specified for up to 600 MeV, allowing high-energy beam capture measurements in FEC2 and transport to the beam dump.

The posthutch beamline is designed to provide transport to the beam dump housed in the main CLARA accelerator hall. A 20° dipole magnet is used to bend the beam to a large aperture yttrium aluminium garnet (YAG) scintillation screen for beam imaging and energy spectrometry. The dispersion at the spectrometer YAG station is modified by a single quadrupole specified to achieve the zero-dispersion condition at the screen position. To optimize the beam imaging, the horizontal and vertical beta functions are minimized at the YAG location, to maximize the energy resolution while also maximizing the image intensity; this is achieved by utilizing the post-IP hutch quadrupoles as part of the dump line matching.

Access to the hutch with the accelerator running is made possible via the interlock of the FEBE arc dipoles to the machine's personal safety system. The total beam power within the hutch is limited to 6.25 W, which offers sufficient flexibility with available bunch charge (maximum 250 pC), bunch repetition rate (maximum 100 Hz), ∼100 TW laser repetition rate (5 Hz) and final beam energy (250–2000 MeV). Radiation shutters on either side of the enclosure (in the CLARA tunnel) are used to shield the hutch from radiation generated from the main CLARA accelerator.

The beam specification at the FEC1 IP is presented in Table I for four possible accelerator configurations. The commissioning target high and low charge modes will form the nominal baseline made available to users from the start of the initial beam exploitation period. Progression toward more demanding parameters including higher peak current and improved transverse quality will be made through periods of machine development. Machine development will also include the development of appropriate diagnostic systems required to verify those parameters [22].

III. START-TO-END SIMULATIONS

Start-to-end simulations were performed to evaluate and optimize the electron beam properties at the FEC1 IP. Simulations targeted machine configurations that deliver one or more beam properties relevant to the anticipated user experiments, including high peak current and charge density. Table I details the four main accelerators operating modes addressed through simulations.

Particle tracking simulations were carried out using ASTRA [23], ELEGANT [24], and GPT [25], accounting for the nonlinear effects (both longitudinal and transverse) of space charge and CSR. The simulation codes were accessed via a Python-based framework (SimFrame) developed at STFC Daresbury Laboratory, which allows a single human-readable lattice file to be deployed consistently across several codes.

ASTRA and GPT were primarily used to simulate the CLARA front end at low energy (below 35 MeV), where transverse and longitudinal space-charge forces are the dominant emittance-diluting processes. Tracking through the injector with 256,000 macroparticles was found to produce a good agreement between codes within a reasonable computation time.

Above 35 MeV, ELEGANT was primarily used due to its processing speed and the inclusion of CSR effects in the bunch compressor and FEBE arc. These high-energy sections (above 35 MeV) of the machine were simulated with 32,000 macroparticles (downsampling the output of the injector simulations); high-fidelity simulations used for machine optimization required 256,000 macroparticles. Extensive comparisons were made between ELEGANT and ASTRA at higher energies, showing small differences due to transverse space-charge effects (not included in ELEGANT) but similar longitudinal space-charge forces. ASTRA does

not include adaptive space-charge meshing, which complicates particle tracking under the bunch-compression scenarios.

Bunch properties (for both low and high-charge configurations in Table I) at the FEC1 IP were inferred from the statistical distribution of particles from tracking simulations. To characterize the longitudinal profile of the bunch, the peak current, current full width at half maximum (FWHM), quarter max (FWQM), and charge fraction (integrated charge within the current FWQM) were extracted. Due to the statistical nature of particle tracking, particularly with space-charge and CSR effects, a smoothing algorithm (kernel density estimation, KDE) was applied to the longitudinal charge distribution. The probability density function and associated cumulative density function were obtained and used to evaluate the full width and charge fraction values. Each configuration was tuned to maximize the peak beam current, which was sensitive to the length of each slice in the time domain and the average number of macroparticles per slice.

For high peak current generation, the most effective accelerator actuators were those modifying the longitudinal phase space of the bunch: the amplitudes and phases of radio-frequency (rf) linacs, wakefield structures (including dielectric energy dechirping), and transverse bending structures that lead to coherent effects like CSR. The FEBE beamline contains only one of these structures, in the form of the FEBE arc and its associated CSR effects, where the arc is designed to minimize the induced CSR kicks, as described in [21]. In principle, the R_{56} of the arc can be adjusted by varying the strengths of the two quad families allowing R_{56} values between ± 20 mm; this, however, produces nonzero dispersion at the exit of the arc. Dispersion cancellation is only achieved with the nominal arc R_{56} of 7.7 mm as noted in Sec. II. The Twiss parameters for the nominal FEBE beamline are shown in Fig. 4.

The main optimization actuators for the FEBE beam are found in the preceding CLARA beamline, shown in Fig. 1.
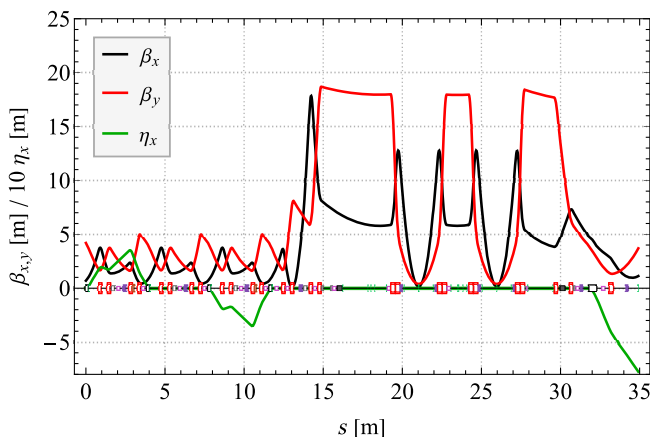
The first 2-m S-band injector linac (Linac 1) can act as either a standard low energy accelerating structure or a longitudinal bunching structure for short single-spike operation [26]. The remaining three 4-m long S-band linacs (Linacs 2–4) provide acceleration up to a nominal beam energy of 250 MeV. A chicane-type VBC is located between Linac 3 and Linac 4, with an X-band 4HC immediately before the VBC for longitudinal phase space curvature compensation. The VBC is located at a nominal energy of ~180 MeV, to maximize its effectiveness for the moderate compression required for the original CLARA FEL concept.

The nominal FEBE arc R_{56} of $+7.7$ mm is of the opposite sign from the main bunch compressor R_{56} of -42 mm. Sextupoles are used to cancel the natural T_{566}. For standard operating modes, the FEBE arc is decompressing for a standard longitudinal chirp. Reversing the chirp using Linac 4 after the VBC is difficult; achieving maximum compression in the FEBE hutch, therefore, requires overcompression in the VBC, followed by recompression during transport in the FEBE arc. This has the additional benefit of reducing the CSR effects in the FEBE arc itself, at the cost of a longitudinal crossover in the VBC.

The CLARA beamline also contains a dielectric-based dechirper structure used to minimize the projected energy spread at the FEL [27]. This device is located a few meters upstream of the FEBE extraction dipole. The dechirper was modeled in ELEGANT as a 1D longitudinal wakefield element using a theoretically calculated Green's function, which has been experimentally verified for this structure [9]. Future work will incorporate full 3D simulations of the wakefield dynamics.

Three different algorithms were used for optimization of the combined CLARA FEBE beamline: A SciPy-based genetic algorithm, a SciPy-based Nelder-Mead simplex algorithm, and a custom-written Nelder-Mead simplex algorithm. The optimization constraints are shown in Table II. At high compression factors, CSR effects can drastically increase the horizontal projected emittance, making beam transport through narrow experimental apertures difficult and restricting the minimum beam focus that can be achieved at each IP [28]. Emittance growth was, therefore, introduced as an additional constraint.

FIG. 4.   Twiss parameters for the full FEBE beamline starting from the first dipole in the FEBE arc.

TABLE II.   Optimization constraints used for particle tracking.

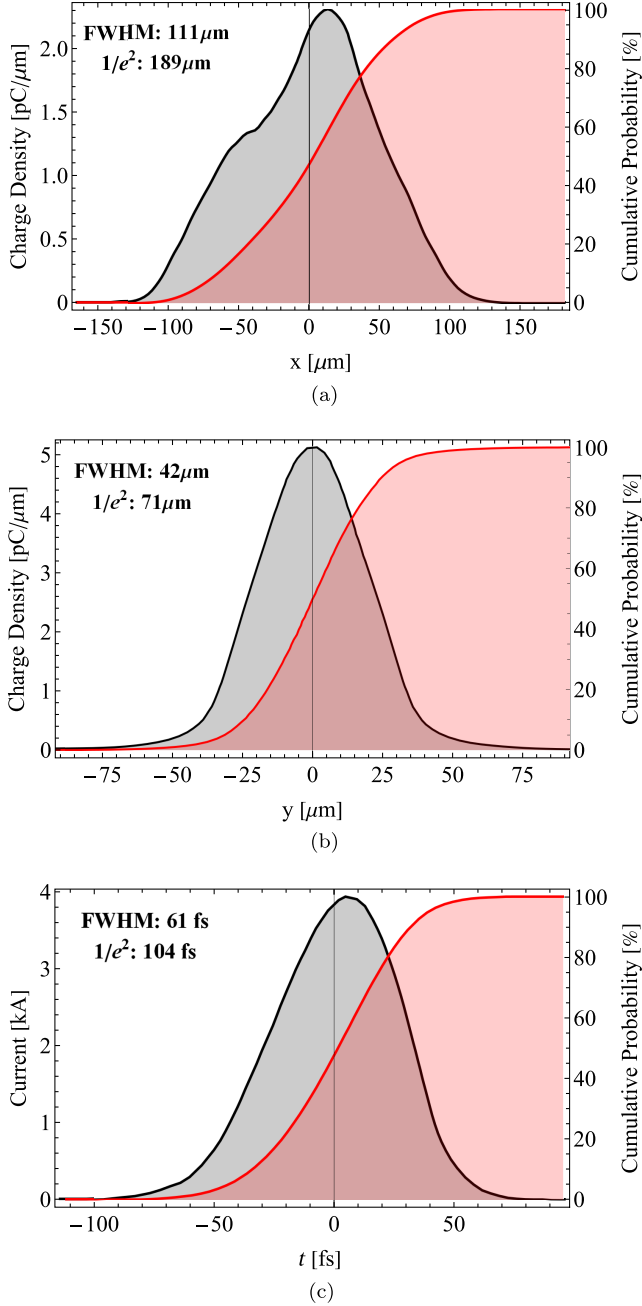| Constraints	Value
Linac gradients	<25 MV/m
Beam energy	240–260 MeV
Peak current @ IP	>2.5 kA
Slice $\epsilon_{N,x}$ @ IP	<10 µm rad
Slice $\epsilon_{N,y}$ @ IP	<1 µm rad
FWQM	0.03 ps
FWQM charge fraction	>75%

FIG. 5. Charge densities and cumulative probability function for an optimized 250 pC solution given at the FEBE FEC1 IP for (a) the transverse horizontal, (b) vertical, and (c) longitudinal planes. Beam parameters extracted from the density functions are presented.

Optimization of the transverse lattice parameters was found to vary with rf focusing from Linacs 1–4. Lattice matching was not performed on an iteration-by-iteration basis, but rematching was conducted when the tracked beta functions strayed too far from design values. In general, re-matching was only performed between optimization sessions. Figure 5 shows projections of the bunch

charge distribution at the FEC1 IP, calculated for the nominal simulation of the high-charge (250 pC) operating mode. This mode corresponds to the "Commissioning: high charge" parameters listed in Table I. We utilize low bandwidth KDE functions to smooth the noisy longitudinal charge distribution and present both the linear charge density and cumulative density functions. Relevant length measurements are shown for each plane, indicating the spatial and temporal dimensions of the distributions.

To evaluate the possibility of microbunching of the bunch longitudinal phase space [29], a semianalytic model [30] was developed to compute the microbunching gain and energy modulation. This model computes the longitudinal space charge and CSR impedance in the drift spaces, linacs, and bunch compressors, using simulated beam parameters at various points. It allows for intrabeam scattering (IBS) effects to be included or excluded to demonstrate the potential impact on the damping of microbunching gain.

The microbunching gain was calculated in stages with CLARA separated into sections. The longitudinal space-charge-induced energy modulation was calculated for each linac and long drift section iteratively, as this parameter depends on the beam energy and beam size. Average values for the transverse beam size were used for each machine section and a linear increase in beam energy applied for the linacs. The final bunching factor at the exit of the VBC (as a function of uncompressed modulation wavelength) was then given by the impedance in the integral summed over all preceding sections. This process was repeated for the remaining linacs, drifts, and the arc compressor.

Microbunching gain is highly dependent on the initial uncorrelated energy spread ($\sigma_{E,0}$), which causes the exponential damping of modulations. ASTRA simulations of the HRRG and Linac 1 were used to determine $\sigma_{E,0} = 1.06$ keV. The gradient and phase of the gun and Linac 1 were set to (−9°, 120 MV/m) and (−16°, 21 MV/m), respectively. The value of $\sigma_{E,0}$ was calculated as the mean value between ±2 ps. A full summary of the main lattice parameters used for the calculation of the microbunching gain factor is shown in Table III.

TABLE III. Beam and lattice parameters used for the computation of the microbunching gain. Beam parameters as calculated after Linac 1, taken from simulation.

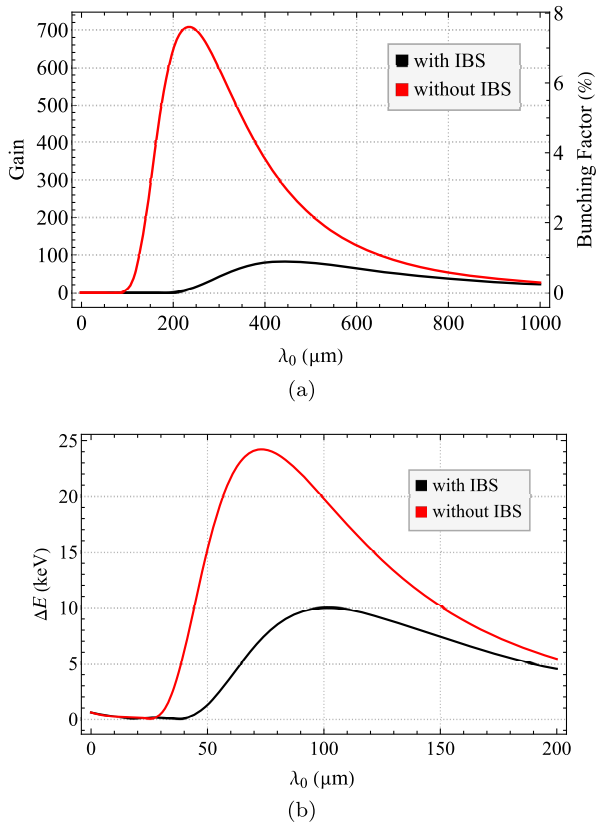| Parameter	Value
Bunch charge (pC)	250
Initial beam energy (MeV)	35
Final beam energy (MeV)	240
Initial uncorrelated energy spread (keV)	1.06
Initial bunch length (ps)	2.42
Initial peak current (kA)	0.05
Normalized emittance (μm rad)	0.42
VBC compression factor	10
Arc compression factor	4

FIG. 6.   Semianalytic model predictions of the (a) microbunching gain and (b) energy modulation amplitude as a function of initial modulation wavelength (λ_0) after compression in both the VBC and the FEBE arc, with and without the energy spread added by intrabeam scattering (IBS).

The output from the semianalytic model is shown in Fig. 6(a), which shows the microbunching gain as a function of the initial modulation wavelength and the final bunching factor, after compression in both the variable bunch compressor and the FEBE arc. Even without including the damping effect caused by IBS, the maximum final bunching factor is around 7%. This level of bunching in the longitudinal plane is expected to be tolerable for most FEBE experiments. The final bunching factor drops by around a factor of 10 when IBS is included.

The energy modulation amplitude is shown in Fig. 6(b). The damping caused by scattering is only around a factor of two at the level of maximum energy modulation, but the calculation without scattering gives this maximum value at approximately 0.1% of the average beam energy (240 MeV).

IV. ACCELERATOR TECHNOLOGY

A. Beam diagnostics

Beam diagnostics for FEBE are designed to verify the targeted commissioning beam parameters as defined in Table I and the requirements of anticipated experiments. The beamline includes an array of well-developed or commercially available diagnostic systems including Ce:YAG screens, stripline beam position monitors, integrated current transformers, and a Faraday cup. An optical transition radiation (OTR) profile monitor located next to the IP aims to measure <10 μm beam sizes expected from plasma accelerators. It has been demonstrated that the resolution could be down to a few μm with an optimized optical system [31]. A diagram showing the location of key diagnostic systems along the FEBE beamline is shown in Fig. 7.

The most demanding requirements on diagnostic systems are set by the beam parameters generated in novel acceleration techniques, including measurement of micrometer-scale transverse profiles, 10 fs bunch duration, emittance, and broadband energy spectra at high resolution. Shot-by-shot characterization is required, particularly in techniques where inherent instabilities may manifest variation of the output beam parameters; noninvasive diagnostics are required for control and optimization. Meeting these challenges has
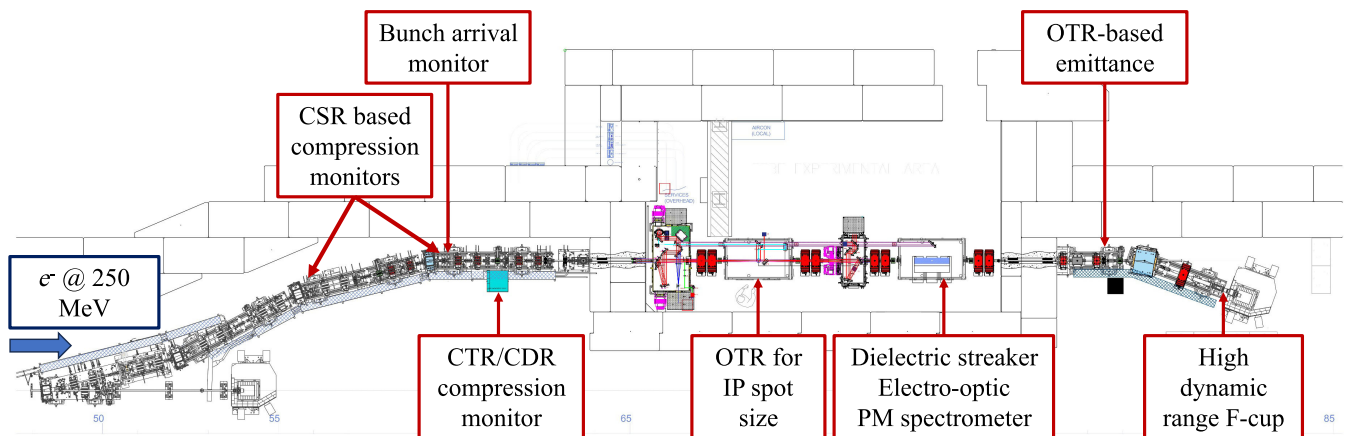

FIG. 7.   Engineering diagram of FEBE beamline, highlighting areas with diagnostic systems undergoing research and development. These areas are supported by standard beam diagnostics including Ce:YAG screens, beam position monitors, and integrated current transformers.

required a dedicated diagnostics R&D program, the key elements of which are detailed below.

1. High dynamic range charge measurement

The flexible beam delivery of FEBE will require both accurate and precise measurements of charges from <5 to 250 pC. Low charge machine setups will be important for the initial phases of some novel acceleration experiments, as the transverse spot sizes and bunch lengths will be significantly lower than at high charge, as shown in Table I. A new electronics front end has been developed for the Faraday cups on CLARA, which will maintain accuracy and a high signal-to-noise ratio across this charge range. This system is comprised of three components: an analog signal chain that converts signals from charge devices into an output pulse proportional to charge; a charge injection circuit for onboard calibration of the analog signal chain; and digital control circuitry to enable operators to adjust the settings of the analog front end. Further details are given in [32].

2. Spectrometer dipole

The FEBE beam line includes an electromagnetic spectrometer for electron beams up to 600 MeV, which can be transported from the FEBE hutch to the beam dump as described in Sec. II. For higher energy beams (e.g., those generated in novel acceleration experiments), an in-vacuum permanent magnet dipole spectrometer has been designed to measure the energy spectra. This spectrometer will nominally be situated in FEC2 and can measure beam energies in the range of 50–2000 MeV, including beams with significant shot-to-shot instabilities and bunches with high-energy spread.

Using a permanent magnet spectrometer within the FEBE hutch simplifies access and minimizes time to reconfigure between experiments. The system is more compact than for an equivalent electromagnet spectrometer and does not require cooling or an additional power supply. The relative compactness of the system allows for the magnet to be removed if not required, and the FEC2 space used for other beam diagnostics.

A long C-core dipole disperses electrons of different energies via the open side onto a long screen. The screen is positioned just below the spectrometer and angled at 45° to allow viewing by cameras positioned in air. The design is modular, consisting of up to five identical sections with lengths of 200 mm which colocate using precision metal dowels. All five sections (total magnet length of 1000 mm) will be used for GeV-scale experiments. A shortened version consisting of three segments at 600 mm total length may be employed for experiments at lower energy gain (≤600 MeV).

The magnetic flux is provided using blocks of neodymium iron boron (NdFeB) with a typical remnant field of 1.41 T and Ni-Cu-Ni coating for vacuum compatibility. Blocks are positioned on either side of the C-core gap by an
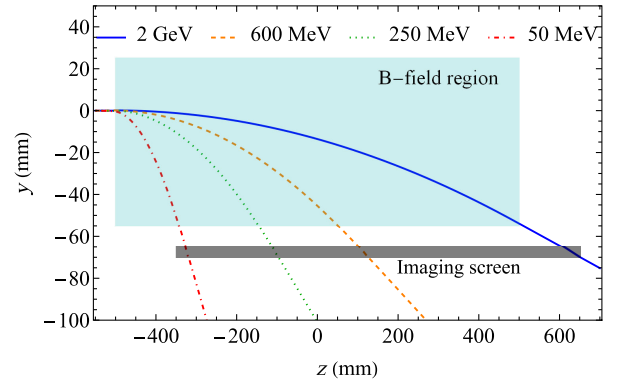

FIG. 8. Plot of the predicted trajectories of electrons in the full energy range through the 1-m-long five-section spectrometer. $z = 0$ is located at the spectrometer midpoint, $y = 0$ is the beam entry height. The region of the magnetic flux is shown in blue between ± 500 mm; trajectories for 2 GeV (solid blue), 600 MeV (orange dashed), 250 MeV (green dotted), and 50 MeV (red dash-dot) are plotted.

aluminum lattice. A total of 80 blocks will be used with dimensions $49 \times 38.5 \times 18$ mm, with a predicted maximum central flux density of 0.72 T. The magnet horizontal aperture is 20 mm which is the maximum size required to maintain a sufficient flux density for GeV-scale use. The predicted trajectories at different electron energies, encompassing a variety of foreseen post-IP beam configurations, are shown in Fig. 8.

The design of the magnet is such that leak fields (evaluated at 0.5 mT for the 1000 mm total length) are well contained above and to the sides of the magnet, extending 150 mm below the open gap and 160 mm beyond the end of the magnet. The magnet is, therefore, not expected to impact of the installation and operation of equipment within FEC1. In addition, the magnet can be translated horizontally out of the main beam path using a motion stage, with the magnet yoke acting to contain the field and shield the beam axis.

3. Longitudinal diagnostics

FEBE will utilize multiple longitudinal diagnostic systems to provide measurements of relative bunch compression, rms bunch length, and detailed longitudinal profile reconstruction.

A bunch compression monitor based on coherent transition radiation will be installed at the end of the FEBE arc. The device uses mesh filters in order to act as a rudimentary spectrometer and provide indicative bunch duration information. The system will operate across a bandwidth of 0.1–5 THz, measuring minimum rms bunch lengths ≲50 fs for charges as low as 100 pC. The detector is a bespoke pyroelectric system, employing variable gain, active noise cancellation, and Winston cones for radiation capture. Both solid and holed (for coherent diffraction radiation, CDR) targets can be used; the latter offers the potential for noninvasive measurements of shot-to-shot compression jitter. The CLARA beamline includes a 9-cell disk-loaded
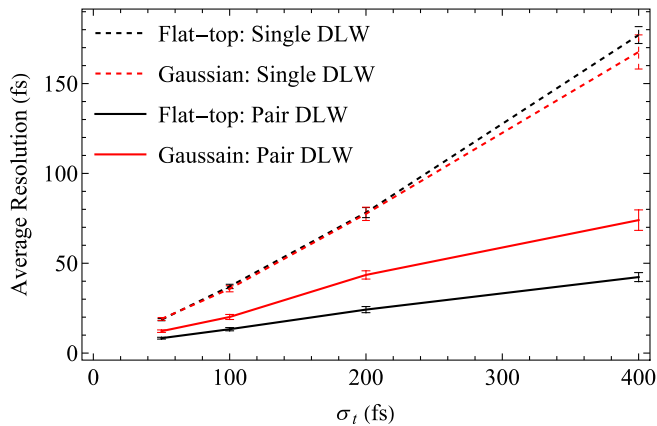
FIG. 9.   Simulated average resolution of the DLW streaker at 250 pC for varying bunch length σ_t for Gaussian (red lines) and flat top (black) profiles, where flat top has a total length of $4\sigma_t$. The improvement in resolution from using a pair of orthogonally oriented structures (solid lines) as compared to a single structure (dashed) is shown.

TDC (position shown in Fig. 1), with up to 10 MV/m integrated transverse voltage and 10 fs slice resolution. Combined with accurate measurements using this upstream TDC, the FEBE bunch compression monitor will ensure maximally compressed beams are delivered for user experiments as required.

A passive streaker based on a dielectric wakefield (DLW) accelerator structure reported in [8] is under the development and will be used to make bunch length measurements across the range of ~50 fs to >1 ps. As compared to the previous design, the FEBE streaker uses two orthogonal waveguides mounted as a pair to compensate for the effect of quadrupolelike wakefields that lead to nonlinear streaking forces; this improves the resolution of the device by a factor of ~3. The simulated resolution as a function of bunch length (at 250 pC) is plotted for single and paired structure arrangements and compared in Fig. 9. The DLW streaker resolution does not scale favorably with reducing beam charge and will not be able to resolve the bunch length at low charges.

Simulations were conducted using the dielectric wakefield and beam tracking software DIWACAT [33]. Wakefields are calculated using the transverse operator method outlined in [34] and results from DIWACAT have been benchmarked against experimental results [8]. The resolution with a passive streaker is a function of the longitudinal position within the bunch, with poor resolution at the head [35]. The average resolution shown in Fig. 9 is given by $\int_{-\infty}^{+\infty} \rho(t) r(t) dt / \int_{-\infty}^{+\infty} \rho(t) dt$, where $\rho(t)$ is the current at longitudinal position t and $r(t)$ is the instantaneous resolution as defined in [35].

The bunch parameters used for these simulations are equal to the machine development parameters listed in Table I, with no beam optics between the end of the streaker and the screen 5 m downstream. In the pure drift case, the resolution does not depend on the distance between the streaker and screen.

The streaker will be located in the FEBE hutch and therefore cannot be directly benchmarked against the TDC (Fig. 1). However, the CLARA beamline contains a dielectric-based dechirper structure (not shown in Fig. 1) that is able to drastically reduce the correlated energy spread (chirp) as demonstrated by simulations [27]. The arc R_{56} would, therefore, have negligible effect on the bunch length thus allowing comparison, albeit indirect, of measurements by the TDC and the streaker. Passive streaker devices based on corrugated wakefield structures were demonstrated to be able to resolve longitudinal bunch profile, including benchmarking against TDC measurements [36,37]; however, dielectric structures in orthogonal geometry need to be investigated which will constitute part of the CLARA beam commissioning.

4. Emittance diagnostics

Single-shot emittance diagnostics will have a high impact in novel acceleration experiments where the potential beam instabilities hinder the application of conventional multishot techniques (e.g., quadrupole scan technique). FEBE will utilize emittance diagnostics based on imaging of optical transition radiation (OTR), which is a well-established technique for measuring transverse beam sizes and beam divergences. As both spatial and angular information from the electron beam is encoded in OTR, a direct measurement of beam emittance is possible: This requires localizing divergence measurements to discrete regions of the spatial OTR image, analogous to making an emittance measurement using a mechanical slit or "pepper-pot." Two techniques are under investigation to produce an OTR-based "optical pepper-pot": Optical masking using a digital micromirror device [38] and imaging with a microlens array [39]. In addition, conventional techniques, i.e., quadrupole and slit scans, will be employed to evaluate the emittance of beams delivered to FEBE.

5. Virtual diagnostics

Machine learning (ML)-based algorithms can be used to predict beam parameters at a given location from a set of input machine parameters that the ML model has been trained on. Such "virtual diagnostics" are particularly relevant in experiments where diagnostics cannot be installed, e.g., due to spatial and mechanical constraints, or where a non-invasive measurement is required but not available [40].

As part of the FEBE design, virtual diagnostics for prediction of the IP beam size have been developed, which make an inference based on an image of the beam either up- or downstream of the IP [41]. This allows, for example, noninvasive measurements of the electron beam to be performed with the FEBE 100 TW laser running through the FEC1 IP, which prevents the insertion of any screen.
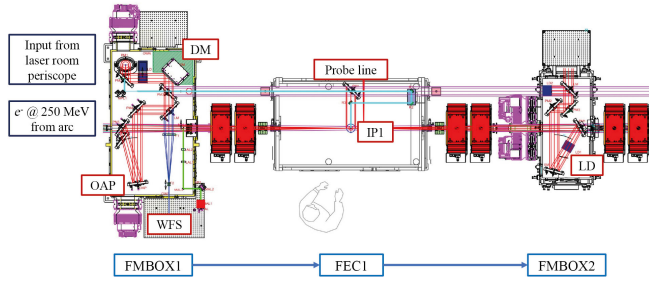
FIG. 10.   Laser transport within the FEBE hutch, with electrons from CLARA traveling FMBOX1-FEC-FMBOX2 (left to right). The laser is brought to a common focus with the electron beam at IP1. OAP: off-axis parabola; IP: interaction point; DM: deformable mirror; WFS: wavefront sensor; and LD: laser dump.

Future development will focus on virtual diagnostics for longitudinal phase space prediction, building upon recent work [42] and utilizing data from the FEBE bunch compression monitor. The use of information in the form of noninvasive shot-to-shot spectral measurements has been shown to improve the accuracy of phase space predictions [43], while recent work based solely on experimental data has demonstrated predictions at significantly higher resolution than previous studies [44].

B. Laser system and laser transport

The FEBE beamline will have access to a high-power (100 TW: ~2.5 J, ~25 fs pulse duration, 5 Hz) Ti:Sapphire laser, which can be combined with the electron beam in FEC1. The laser requirements are compatible with the demands of plasma acceleration and can be used for ionization and/or wakefield excitation.

The laser system including the vacuum compressor is housed in a dedicated laser room immediately on top of the FEBE hutch. Light from the compressor is transported in vacuum from the laser room to the hutch via a radiation-shielded periscope; this allows personnel to access the laser room while the electron beam is in the FEBE hutch. The laser transport system inside the hutch is shown in Fig. 10 and facilitates two primary transport arrangements: (1) collinear propagation of laser light with the electron beam to a focus in FEC1 and (2) delivery of the laser without focusing directly to FEC1 for general exploitation, which can also be used for a probe line.

Laser focusing on the collinear path is achieved using a ~3.5-m off-axis parabola housed in FMBOX1, with laser and electron beam combined on a holed mirror. This is the longest focus that can be generated while keeping the laser within the footprint of the FEBE hutch. The mirror box includes an adaptive optic system for focal spot optimization, consisting of a deformable mirror and wavefront sensor mounted at the conjugate plane to the deformable mirror. Leakage paths into air will be utilized for other laser diagnostics, including shot-by-shot measurements of pulse energy, spectrum, and beam pointing. The laser is allowed

to expand after the focus to a safe intensity before being separated from the electron beam using a holed mirror in FMBOX2, which also includes space for laser exit mode diagnostics and laser termination.

C. Timing and synchronization

FEBE laser synchronization will be performed using systems developed for other systems on CLARA, aiming to deliver <10 fs laser-electron beam synchronization. The timing architecture is similar to that employed at larger x-ray FEL facilities [45] and is split into three key systems. (i) Ultrastable optical clock based on a commercial low-noise fiber laser system (1560 nm, 250 MHz Er/Yb fiber oscillator; Origami, OneFive), phase-locked to an rf master oscillator for long-term stability. (ii) The CLARA stabilized the optical timing network to deliver the optical clock to several clients on the accelerator, with active correction of the fiber length via measurement of the round-trip time. (iii) End-station synchronization (repetition rate locking) to the optical clock, including laser-laser (via optical cross-correlation), and laser-rf synchronization.

Two stabilized links will be routed from the CLARA optical timing network to the FEBE beamline: one for synchronization of the 100 TW laser and a second for a bunch arrival-time monitor (BAM).

To improve the synchronization of the laser, a two-color balanced optical cross-correlator (TC-BOXC) based on periodically poled lithium niobate waveguide [46] has been developed. The TC-BOXC will be used to lock the FEBE laser master oscillator to the CLARA optical timing network. Repetition rate locking will be based on a hybrid locking configuration that uses an rf mixer and photodetector to perform coarse locking prior to locking the laser with the more sensitive TC-BOXC.

The waveguide-based TC-BOXC has a measured sensitivity of 0.97 mV/fs and a theoretical resolution of 4.2 mV/fs. The theoretical resolution of this device provides an order of magnitude improvement over conventional bulk crystal cross correlators. The TC-BOXC is an all-fiber device that is more robust against environmental fluctuations and requires less (valuable) optical table space compared to its free-space counterpart.

The BAM will be based on a PCB substrate with rod-shaped pick-ups in a similar design to [47]. The initial performance target is 10 fs resolution for bunch charges as low as <5 pC. Initial tests are expected to be performed with the BAM mounted within FEC2.

D. Vacuum management

The FEBE vacuum design accommodates a wide range of possible experiments. Of these experiments, those targeting plasma acceleration are the most demanding on vacuum the management due to the associated gas injection at high pressure.

The FEBE design transfers vacuum management to outside of the experiment chambers by introducing aperture restrictions throughout the FEBE beamline. This provides maximum flexibility to the user as required, however, this results in the gas particles propagating up- and downstream of the source. This increases the pressure in the FEBE arc and main CLARA accelerator above nominal levels.

High gas pressures lead to strong beam-gas scattering effects which increase the electron beam normalized emittance. Following the work in [48], we have assessed the effects of high gas loading on beam emittance for representative experimental gas profiles. The approach utilized modeled Twiss parameters throughout the line via linear interpolation; the gas profile was built from a series of defined pressure points and was similarly interpolated. The incoming horizontal and vertical electron beam emittances were 5 and 0.4 μm rad. The assessment is performed for 0.01 mbar of gas pressure at the IP (worst case estimate, based on a gas jet positioned at $z = 0$ m with 100 bar backing pressure and 100 ms opening time), with various aperture restrictions in the FEC1, as well as beam apertures in FMBOX1/2 due to mirrors.

Simulations were performed using MolFlow [49]. These demonstrate $\sim 10^{-6}$ mbar at the beam shutter on the outside wall of the FEBE hutch. The impact of hydrogen and argon gas species were compared. Figure 11 shows the gas density profile and matched beta-functions for the FEBE beamline between the dipole magnet and the end of the hutch, and the vertical normalized emittance for both gas species. As expected, due to the higher molecular weight,
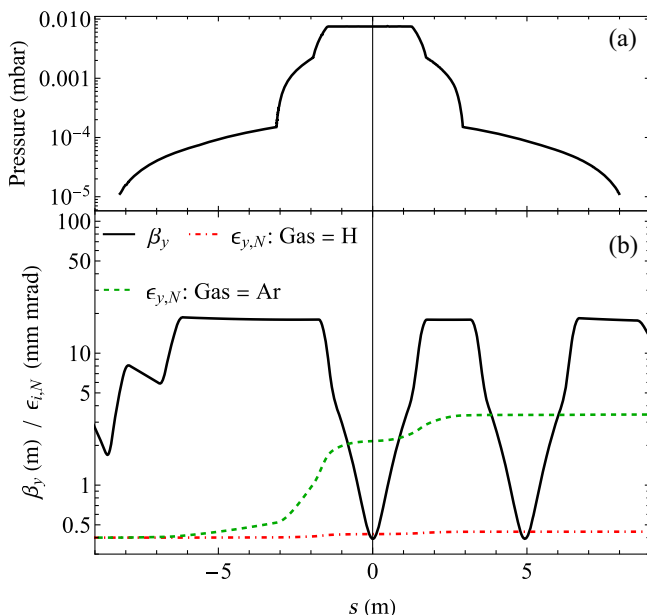

FIG. 11.   (a) Gas pressure profile for hydrogen and argon and (b) normalized vertical emittance and vertical beta functions ± 10 m from the FEC1 IP (located at $s = 0$ m). Base gas pressure of 0.01 mbar at the IP is assumed, with a pressure reduction to 10^{-6} mbar at either end of the vacuum line.

there is a significant increase in emittance for argon as compared to hydrogen. The vertical emittance increases by almost an order of magnitude, primarily due to the combination of relatively high beta function and gas pressure seen between FMBOX1 and the IP. Emittance blow-up inside the FEC1 chamber is minimal as the transverse beta functions rapidly decrease in this region. Due to the significantly larger expected horizontal emittance for these experiments, ~ 5 mm mrad, only small changes are seen in the horizontal plane.

The vacuum management system will be updated following the results of initial operations and testing of gas targets. Should gas loading exceed expected values in practice, an alternative design solution based on management close to the target (similar to as deployed by [50]) will be used.

For conducting in-air experiments, e.g., irradiation for VHEE experiments, a beryllium window of thickness 250 μm will be installed at the beginning and exit of the chamber. The degradation to the beam quality due to this window is expected to be within the tolerance of user requirements, however, detailed simulations will be conducted by relevant users to verify this and account for any impact.

E. Longitudinal profile shaping

Optimization of the longitudinal profile of the photoinjector laser provides two key benefits to electron beam optics. The first benefit is flexible variation and correction of the laser profile to improve the electron bunch longitudinal and transverse optics and mitigate space charge and other collective effects in the beam transport. The second benefit is the modification of the longitudinal profile to maximize the potential of novel acceleration experiments [51,52]. The capability to shape the longitudinal profile of electron bunches has therefore been developed for use in FEBE and, while predominantly targeted to drive-witness wakefield beam experiments, will be made available to all users. Longitudinal laser shaping is performed via control of the photoinjector laser profile [53] and can be used either standalone or in combination with other methods described in Secs. II and III, including the use of the mask installed in the FEBE arc.

Control of the photoinjector laser is performed using an acousto-optic modulator integrated into a 4-f spectral filter [54]. To shape the laser pulse temporally, the spectral phase of the pulse can be adjusted by varying the temporal phase of the acoustic wave (created using an rf pulse generator) which drives the modulator. Pulses can also be shaped temporally by varying the temporal amplitude of the acoustic wave, however, this approach reduces the output pulse energy and is undesirable when maintaining high-charge operation from the photoinjector.

In order to produce a particular target pulse temporal intensity profile, a suitable spectral phase mask must first be identified. This is nontrivial for arbitrary shapes, requiring full knowledge of both the phase and amplitude in either the spectral or temporal domain to fully define the pulse.
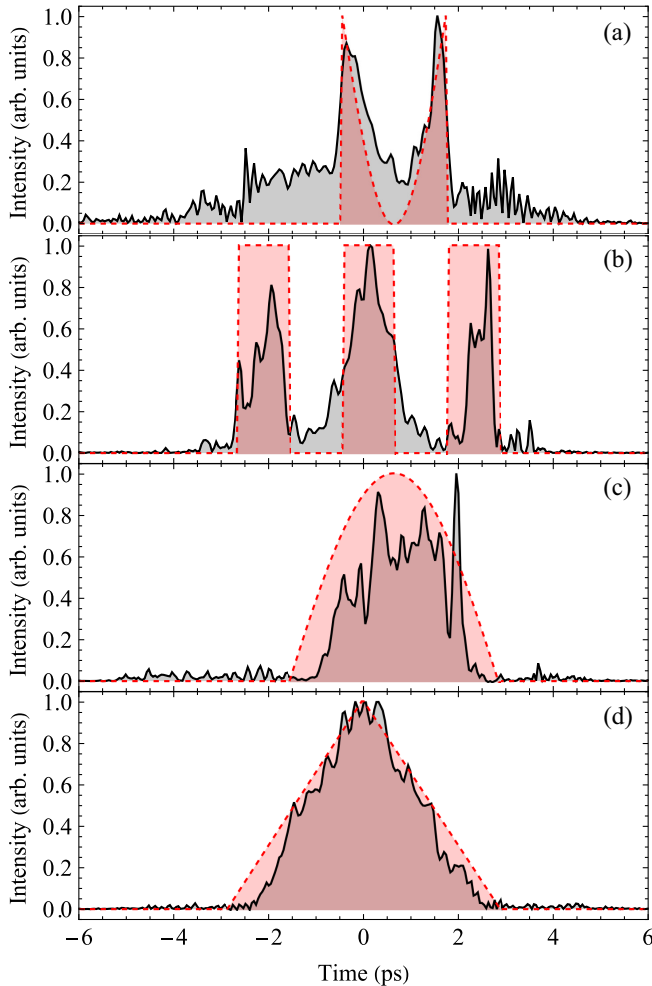
FIG. 12. Demonstration of solutions to deliver arbitrary photo-injector laser temporal profiles via spectral phase manipulation, comparing target (red dashed lines), and predicted (black solid) profiles. Results for different profiles are compared, including: (a) double ramp, (b) triple flat top, (c) cut sine wave, and (d) triangular.

With only the temporal and the spectral intensity fully known, a suitable phase mask must be identified to fully specify the output pulse.

For maximum flexibility and rapid customisation, an ML model has been developed to find the required phase mask to achieve a (user defined) target pulse temporal profile. Training data were generated from 10^6 pairs of simulated spectral phase profiles and matched temporal intensity profiles, with a further 10^5 pairs generated for the test dataset. To encode the physical limitation of the acousto-optic modulator bandwidth into the network, the model includes a regularizer that acts to limit the gradient of the spectral phase profile to within physical limits. High-quality (and physically realizable) matches to target have been achieved for a range of pulse profiles, as shown in Fig. 12. The system will in future be trained using live data to explore and account for expected deviations between simulation and practice.

Deployment of the ML system for control of the laser pulse shape has begun, with machine operators able to specify arbitrary pulse shapes for which the ML system produces an appropriate spectral phase profile. This generated profile is then sent to the laser control system and applied to the acousto-optic modulator, with a total time between user request and laser activation of less than 100 ms.

V. SUMMARY

A new beamline for full energy beam exploitation (FEBE) has been designed and is currently undergoing installation on the CLARA test facility at STFC Daresbury Laboratory. The goal of this beamline is to support a wide variety of user-driven experiments utilizing 250 MeV ultrabright electron bunches delivered at repetition rates up to 100 Hz. The beamline incorporates two large-volume experiment chambers with a shielded user hutch, for ease of user access and flexibility in setup of novel experiment apparatus.

A key component of the foreseen future experiment program is a novel acceleration, with expressions of interest for plasma acceleration (laser- and beam-driven) and structure wakefield acceleration. This has driven key components of the beamline design, including beam diagnostics for GeV scale, 10 fs duration, and micrometer-scale transverse profile electron bunches. The beamline includes the infrastructure for combining electron bunches with a high-power (100 TW) laser, housed immediately above the beamline and brought into the hutch via a dedicated vacuum laser transport. The laser will be synchronized to the CLARA bunches using an optical timing architecture similar to those used at larger x-ray FEL facilities.

CLARA will exit shutdown for installation of accelerator modules in the third quarter of 2023 and will proceed to enter a period of technical and machine commissioning running through to the second half of 2024; installation and commissioning of the 100 TW laser will then take place, running through to early 2025. An open call to the community is expected to be issued in mid-2024 for beam time early 2025 but will be contingent on the results of the machine commissioning. Future operations are expected to be divided between the user access and ongoing machine development. The machine development will focus on achieving more challenging electron bunch parameters and configurations, as well as improving reliability in beam delivery. Time will also be used to ensure CLARA can continue to be a testing ground for future UK accelerator facilities, such as UK XFEL [55,56].

[1] J. Clarke, D. Angal-Kalinin, N. Bliss, R. Buckley, S. Buckley, R. Cash *et al.*, CLARA conceptual design report, J. Instrum. **9**, T05001 (2014).

[2] D. Angal-Kalinin, A. Bainbridge, A. D. Brynes, R. K. Buckley, S. R. Buckley, G. C. Burt *et al.*, Design, specifications, and first beam measurements of the compact

linear accelerator for research and applications front end, Phys. Rev. Accel. Beams 23, 044801 (2020).

[3] J. McKenzie, P. Goudket, T. Jones, B. Militsyn, L. Cowie, G. Burt, and V. Paramonov, High repetition rate s-band photoinjector design for the CLARA FEL, in Proceedings of the 36th International Free Electron Laser Conference, FEL-2014, Basel, Switzerland (JACoW, Geneva, Switzerland, 2014).

[4] A. Brynes, S. Jamison, B. Muratori, N. Thompson, and P. Williams, Laser heater design for the CLARA FEL test facility, in Proceedings of the 8th International Particle Accelerator Conference, IPAC-2017, Copenhagen, Denmark (JACoW, Geneva, Switzerland, 2017).

[5] T. H. Pacey, Y. Saveliev, A. Healy, P. G. Huggard, B. Alderman, P. Karataev, K. Fedorov, and G. Xia, Continuously tunable narrow-band terahertz generation with a dielectric lined waveguide driven by short electron bunches, Phys. Rev. Accel. Beams 22, 091302 (2019).

[6] K. L. Small, N. T. Henthorn, D. Angal-Kalinin, A. L. Chadwick, E. Santina, A. Aitkenhead et al., Evaluating very high energy electron RBE from nano-dosimetric pBR322 plasmid DNA damage, Sci. Rep. 11, 3341 (2021).

[7] M. Hibberd, A. L. Healy, D. S. Lake, V. Georgiadis, E. J. H. Smith, O. J. Finlay et al., Acceleration of relativistic beams using laser-generated terahertz pulses, Nat. Photonics 14, 755 (2020).

[8] Y. M. Saveliev, T. H. Pacey, J. K. Jones, and G. Xia, First dielectric wakefield experiments at Daresbury Laboratory, J. Phys. Conf. Ser. 1596, 012015 (2020).

[9] Y. Saveliev, T. J. Overton, T. H. Pacey, N. Joshi, S. Mathisen, B. D. Muratori, N. Thompson, M. P. King, and G. Xia, Experimental study of transverse effects in planar dielectric wakefield accelerating structures with elliptical beams, Phys. Rev. Accel. Beams 25, 081302 (2022).

[10] D. Angal-Kalinin, J. K. Jones, T. Pacey, R. Corsini, F. Burkart, R. Pompili, F. Stephan, X. Li, A.-S. Müller, and M. Schuh, Electron beam test facilities for novel applications, in Proceedings of the 14th International Particle Accelerator Conference, IPAC-2023, Venice, Italy (JACoW, Geneva, Switzerland, 2023).

[11] CERN linear electron accelerator for research, http://clear.cern/.

[12] R. Corsini, W. Farabolini, A. Malyzhenkov, A. Dyks, P. Korysko, K. Sjobak, and V. Rieker, Status of the CLEAR user facility at CERN and its experiments, in Proceedings of the 31st Linear Accelerator Conference, LINAC-2022, Liverpool, United Kingdom (JACoW, Geneva, Switzerland, 2022).

[13] Accelerator research experiment at SINBAD, https://ares.desy.de/.

[14] F. Burkart, R. Assmann, H. Dinter, S. Jaster-Merz, W. Kuropka, F. Mayet, B. Stacey, and T. Vinatier, The ARES Linac at DESY, in Proceedings of the 31st Linear Accelerator Conference, LINAC-2022, Liverpool, United Kingdom (JACoW, Geneva, Switzerland, 2022).

[15] Sources for plasma accelerators and radiation Compton with laser and beam, https://sparclab.lnf.infn.it/.

[16] F. G. Bisesto, M. P. Anania, M. Bellaveglia, E. Chiadroni, A. Cianchi, G. Costa et al., The FLAME laser at SPARC_LAB, Nucl. Instrum. Methods Phys. Res., Sect. A 909, 452 (2018).

[17] A. F. Habib, G. G. Manahan, P. Scherkl, T. Heinemann, A. Sutherland, R. Altuiri et al., Attosecond-Angstrom free-electron-laser towards the cold beam limit, Nat. Commun. 14, 1054 (2023).

[18] Y. Wu, J. Hua, Z. Zhou, J. Zhang, S. Liu, B. Peng et al., High-throughput injection–acceleration of electron bunches from a linear accelerator to a laser wakefield accelerator, Nat. Phys. 17, 801 (2021).

[19] C. Emma, J. V. Tilborg, R. Assmann, S. Barber, A. Cianchi, S. Corde et al., Free electron lasers driven by plasma accelerators: Status and near-term prospects, High Power Laser Sci. Eng. 9, e57 (2021).

[20] M. C. Downer, R. Zgadzaj, A. Debus, U. Schramm, and M. C. Kaluza, Diagnostics for plasma-based electron accelerators, Rev. Mod. Phys. 90, 035002 (2018).

[21] S. Di Mitri, M. Cornacchia, and S. Spampinati, Cancellation of coherent synchrotron radiation kicks with optics balance, Phys. Rev. Lett. 110, 014801 (2013).

[22] T. Pacey, D. Angal-Kalinin, A. Bainbridge, J. Henderson, J. Jones, J. N. Y. et al., Development of a 6d electron beam diagnostics suite for novel acceleration experiments at FEBE on CLARA, in Proceedings of the 11th International Beam Instrumentation Conference, IBIC-2022, Cracow, Poland (JACoW, Geneva, Switzerland, 2022).

[23] K. Floetmann, ASTRA, https://www.desy.de/~mpyflo/.

[24] M. Borland, ELEGANT: A flexible SDDS-compliant code for accelerator simulation, in Proceedings of the 6th International Computational Accelerator Physics Conference, ICAP-2000, Darmstadt, Germany (Darmstadt University of Technology, Darmstadt, Germany, 2000).

[25] Pulsar Physics, General Particle Tracer, http://www.pulsar.nl/gpt.

[26] L. Serafini and M. Ferrario, Velocity bunching in photoinjectors, AIP Conf. Proc. 581, 87 (2001).

[27] M. Colling, T. Pacey, Y. Saveliev, B. Fell, and D. Dunning, Mechanical design of a dielectric wakefield dechriper system for CLARA, in Proceedings of the 10th International Particle Accelerator Conference, IPAC-2019, Melbourne, Australia (JACoW, Geneva, Switzerland, 2019).

[28] A. D. Brynes, P. Smorenburg, I. Akkermans, E. Allaria, L. Badano, S. Brussaard et al., Beyond the limits of 1D coherent synchrotron radiation, New J. Phys. 20, 073035 (2018).

[29] E. Saldin, E. Schneidmiller, and M. Yurkov, Longitudinal space charge-driven microbunching instability in the TESLA Test Facility linac, Nucl. Instrum. Methods Phys. Res., Sect. A 528, 355 (2004).

[30] S. D. Mitri, G. Perosa, A. Brynes, I. Setija, S. Spampinati, P. H. Williams et al., Experimental evidence of intrabeam scattering in a free-electron laser driver, New J. Phys. 22, 083053 (2020).

[31] M. Ross, S. Anderson, J. Frisch, K. Jobe, D. McCormick, B. McKee et al., Very high resolution optical transition radiation beam profile monitor, AIP Conf. Proc. 648, 237 (2002).

[32] S. Mathisen, T. Pacey, and R. Smith, Analog front end for measuring 1 to 250 pC bunch charge at CLARA, in Proceedings of the 11th International Beam Instrumentation

Conference, IBIC-2022, Krakow, Poland (JACoW, Geneva, Switzerland, 2022).

[33] T. Overton, tobyoverton/DiWaCAT: DiWaCAT v0, 10.5281/zenodo.8321426.

[34] S. S. Baturin, I. L. Sheinman, A. M. Altmark, and A. D. Kanareykin, Transverse operator method for wakefields in a rectangular dielectric loaded accelerating structure, Phys. Rev. ST Accel. Beams **16,** 051302 (2013).

[35] P. Craievich and A. A. Lutman, Effects of the quadrupole wakefields in a passive streaker, Nucl. Instrum. Methods Phys. Res., Sect. A **865,** 55 (2017).

[36] J. Seok, M. Chung, H.-S. Kang, C.-K. Min, and D. Na, Use of a corrugated beam pipe as a passive deflector for bunch length measurements, Phys. Rev. Accel. Beams **21,** 022801 (2018).

[37] P. Dijkstal, A. Malyzhenkov, P. Craievich, E. Ferrari, R. Ganter, S. Reiche, T. Schietinger, P. Juranić, and E. Prat, Self-synchronized and cost-effective time-resolved measurements at x-ray free-electron lasers with femtosecond resolution, Phys. Rev. Res. **4,** 013017 (2022).

[38] G. P. LeSage, T. E. Cowan, R. B. Fiorito, and D. W. Rule, Transverse phase space mapping of relativistic electron beams using optical transition radiation, Phys. Rev. ST Accel. Beams **2,** 122802 (1999).

[39] F. G. Bisesto, M. P. Anania, M. Botton, M. Castellano, E. Chiadroni, A. Cianchi *et al.*, Recent studies on single-shot diagnostics for plasma accelerators at SPARC_LAB, Nucl. Instrum. Methods Phys. Res., Sect. A **909,** 364 (2018).

[40] J. Wolfenden, C. Welsch, C. Swain, and T. Pacey, Optical Pepper-pots: Developing single-shot emittance diagnostics, in *Proceedings of the 14th International Particle Accelerator Conference, IPAC-2023, Venice, Italy* (JACoW, Geneva, Switzerland, 2023).

[41] J. Wolfenden, C. Swain, C. Welsch, T. Pacey, A. Pollard, J. Jones, and D. Dunning, Application of virtual diagnostics in the FEBE CLARA user area, in *Proceedings of the 31st Linear Accelerator Conference, LINAC-2022, Liverpool, United Kingdom* (JACoW, Geneva, Switzerland, 2022).

[42] M. Maheshwari, D. Dunning, J. Jones, M. King, H. Kockelbergh, and A. Pollard, Prediction and clustering of longitudinal phase space images and machine parameters using neural networks and K-means algorithm, in *Proceedings of the 12th International Particle Accelerator Conference, IPAC-2021, Campinas, SP, Brazil* (JACoW, Geneva, Switzerland, 2021).

[43] A. Hanuka, C. Emma, T. Maxwell, A. S. Fisher, B. Jacobson, M. J. Hogan, and Z. Huang, Accurate and confident prediction of electron beam longitudinal properties using spectral virtual diagnostics, Sci. Rep. **11,** 2945 (2021).

[44] J. Zhu, Y. Chen, F. Brinker, W. Decking, S. Tomin, and H. Schlarb, High-fidelity prediction of megapixel longitudinal phase-space images of electron beams using encoder-decoder neural networks, Phys. Rev. Appl. **16,** 024005 (2021).

[45] S. Schulz *et al.*, Femtosecond all-optical synchronization of an X-ray free-electron laser, Nat. Commun. **6,** 5938 (2015).

[46] J. Christie, L. Corner, J. Henderson, and E. Snedden, Developing a two-colour all-fibre balanced optical cross-correlator for sub-femtosecond synchronisation, in *Proceedings of the 14th International Particle Accelerator Conference, IPAC-2023, Venice, Italy* (JACoW, Geneva, Switzerland, 2023).

[47] B. Scheible, W. Ackermann, M. Czwalinna, H. D. Gersem, S. Mattiello, A. Penirschke, and H. Schlarb, Bunch arrival-time measurement with rod-shaped pickups on a printed circuit board for x-ray free-electron lasers, in *Proceedings of the 10th International Beam Instrumentation Conference, IBIC-2021, Pohang, Republic of Korea, 2021* (JACoW, Geneva, Switzerland, 2021).

[48] F. L. Pimpec and T. Schietinger, Emittance growth by beam-gas scattering in single pass accelerator, arXiv:1405.1078.

[49] CERN, MolFlow, https://molflow.web.cern.ch/.

[50] N. Delbos, C. Werle, I. Dornmair, T. Eichner, L. Hüber, S. Jalas *et al.*, Lux – A laser–plasma driven undulator beamline, Nucl. Instrum. Methods Phys. Res., Sect. A **909,** 318 (2018).

[51] V. Shpakov, M. P. Anania, M. Bellaveglia, A. Biagioni, F. Bisesto, F. Cardelli *et al.*, Longitudinal phase-space manipulation with beam-driven plasma wakefields, Phys. Rev. Lett. **122,** 114801 (2019).

[52] F. Lemery and P. Piot, Tailored electron bunches with smooth current profiles for enhanced transformer ratios in beam-driven acceleration, Phys. Rev. ST Accel. Beams **18,** 081301 (2015).

[53] A. Pollard, D. Dunning, W. Okell, and E. Snedden, Machine Learning Approach to Temporal Pulse Shaping for the Photoinjector Laser at CLARA, in *Proceedings of the 13th International Particle Accelerator Conference, IPAC-2022, Bangkok, Thailand* (JACoW, Geneva, Switzerland, 2022).

[54] C. W. Hillegas, J. X. Tull, D. Goswami, D. Strickland, and W. S. Warren, Femtosecond laser pulse shaping by use of microsecond radio-frequency pulses, Opt. Lett. **19,** 737 (1994).

[55] UK XFEL: Scientific case project, http://xfel.ac.uk/.

[56] D. Dunning, P. Aden, D. Angal-Kalinin, J. Clarke, J. Collier, B. Fell *et al.*, An introduction to the UK XFEL conceptual design and options analysis, in *Proceedings of the 14th International Particle Accelerator Conference, IPAC-2023, Venice, Italy* (JACoW, Geneva, Switzerland, 2023).